POLITECNICO DI TORINO
Repository ISTITUZIONALE

Unexpected Transient Dynamics of Meandering Rivers With Unsteady Flows

(Article begins on next page)

13 March 2025

Unexpected Transient Dynamics of Meandering Rivers With Unsteady Flows

Francesca Bassani[1,2] ⓘ, Matteo B. Bertagni[2,3,4] ⓘ, Luca Ridolfi[2] ⓘ, and Carlo Camporeale[2] ⓘ

[1]Laboratory of Catchment Hydrology and Geomorphology, École Polytechnique Fédérale de Lausanne, Sion, Switzerland, [2]Department of Environment, Land and Infrastructure Engineering, Politecnico di Torino, Torino, Italy, [3]The High Meadows Environmental Institute, Princeton University, Princeton, NJ, USA, [4]Department of Civil and Environmental Engineering, Princeton University, Princeton, NJ, USA

Abstract River meandering dynamics are here explored in light of unsteady water flows. While mathematical models have usually focused on constant discharges—a reasonable and widely adopted approach for long-term considerations—we show that varying flows strongly affect the short-term planimetric evolution of meanders, before the cutoff occurrence. In particular, flow variability slows down the meanders' dynamics while does not significantly influence the wavelength selection. We support our arguments with numerical simulations and theoretical (linear and nonlinear) analyses, showing that an interplay between out-of-phase river geometry and flow is responsible for the meander-dynamics slowdown. Our results suggest that accounting for flow variability is critical in assessing yearly to decadal meander dynamics with important implications for river engineering and management strategies.

Plain Language Summary Meandering rivers are natural sinuous channels shaping the Earth's surface with their lateral migration motion. Beyond theoretical interest, the investigation of such dynamics is fundamental for river management and restoration. A common way to study river meander dynamics is through numerical simulations that simulate the planform evolution of the river geometry in space and time. A classic assumption in these simulations is a constant water flow. In this study, we show that considering more realistic temporally varying flow discharges slows down the meander growth compared to the case with a constant flow discharge.

1. Introduction

The fascinating dynamics of meandering rivers have been widely investigated during the past decades, not only because of their intrinsic beauty and frequent occurrence in nature but also for their key role in river engineering, management, and restoration (Buijse et al., 2002; Jansen et al., 1979; Ollero, 2010). Typically, morphodynamic models have represented a powerful tool to address and describe the physical mechanisms underlying the meandering dynamics (Camporeale et al., 2007), that is, how the interplay of water flow, sediment load, channel planform, and bed morphology determine the fluvial spatio-temporal evolution. Enhanced by the cooperative advances in geomorphology and fluid dynamics (Seminara, 2006), robust analytical frameworks for flow field and bed topography have been developed (Duan & Julien, 2005; Eke et al., 2014; Ikeda et al., 1981; Imran et al., 1999; Johannesson & Parker, 1989; Parker et al., 2011; Zolezzi & Seminara, 2001). Despite the different mathematical formulations and hypotheses distinguishing these models, a constant water discharge is usually assumed for the flow field. This assumption of a steady component of the forcing, which is also referred to as 'formative' discharge (Inglis, 1949), is grounded in the tenet that a single, dominant flow (arguably related to its sediment transport capability) may determine river channel morphology (quasi-steady morphodynamics, e.g., Pittaluga & Seminara, 2011). In fact, statistical properties of the reach planimetry mainly depend on the dominant flow and fluctuate without changing relevantly with respect to dominant flow-induced morphology (Howard & Hemberger, 1991). Determining whether the equilibrium state under steady forcing is representative of river dynamics, especially at different evolution periods, remains unresolved.

Actually, rivers are far from being steady forced systems: they experience stochastic flows due to the natural fluctuations of the hydrologic forcing. Studies on river eco-morphodynamics have shown that different hydrologic regimes strongly affect the formation and suppression of alternate bars (Carlin et al., 2021; Eekhout et al., 2013; Hall, 2004; Tubino, 1991; Welford, 1994) and the growth of riparian vegetation (Bertagni et al., 2018; Vesipa et al., 2017). Only a few notable studies have explored the impact of stochastic flows on river planar geometry.

Writing – original draft:
Francesca Bassani
Writing – review & editing:
Francesca Bassani, Matteo B. Bertagni,
Luca Ridolfi, Carlo Camporeale

Pittaluga and Seminara (2011) found that different peak discharges affect the river bed scour and deposit. The study highlighted that differences in bed elevation emerge at short-term timescales under varying flow, but concluded that repeated flood sequences (a proxy for unsteadiness) result in a dynamic equilibrium of the system in the long term. The model of Asahi et al. (2013) further demonstrated that flow unsteadiness affects the river planform shape (e.g., width and sinuosity), and bank erosional and depositional processes in meandering rivers. However, a more in-depth understanding of the meandering dynamics under varying flows—from both the riparian geomorphology and hydraulic geometry perspectives—is still missing. Particular attention is also required in light of the extreme events that rivers will increasingly be exposed to (Eccles et al., 2019; François et al., 2019).

Previous works have addressed the problem of variable discharges by accounting for a set of flows that occur intermittently over time (Paola et al., 1992; Parker et al., 1998). Here, we go beyond such simplification by directly considering the probabilistic distribution of unsteady flows to explore their effects on meandering river dynamics. In particular, we focus on the stream planform evolution at short-term timescales, defined as periods shorter than the typical timescale for cutoff occurrence (*sensu* Camporeale et al., 2005). Short-term dynamics are of interest because (a) they can reveal better insights into the meander geometry evolution, without being compromised by the filtering action on geometric nonlinearities induced by cutoff events (Camporeale et al., 2008; Perucca et al., 2005), and (b) they are crucial for engineering purposes and restoration practices given their yearly to decadal timescales (e.g., Ciotti et al., 2021; Gilvear, 1999). To assess the impact of flow variability, we perform short-term numerical simulations of meandering rivers with two models of different complexity, using parameters typical of realistic meandering rivers in nature. By comparing the morphodynamic evolution resulting from constant and unsteady flows, we find that flow variability slows down the planar evolution of the meanders and impacts the meander wavelength. We also perform analytical linear and nonlinear analyses to physically explain the reasons behind such behavior. Our work highlights short-term features that did not emerge in previous constant-discharge analyses and should be considered when developing river engineering and restoration plans.

2. Observations From Short-Term Numerical Simulations

We explore the effects of flow variability on river meander dynamics through a physically based numerical approach. Specifically, we use the seminal model for the river centerline evolution, originally proposed by Hasegawa (1977) and Ikeda et al. (1981) and here referred to as the HIPS model following Parker et al. (2011). Although this model does not account for the riverbed morphodynamics, it has been widely employed in the literature for its conceptual simplicity, robustness, and capability of reproducing the key elements of meandering dynamics: (a) wavelength selection; (b) downstream meander migration; (c) meander elongation; and (d) upstream skewness of meanders (Camporeale et al., 2007). These features allow us to catch the essentials enclosed in the physical interpretation of the phenomena occurring when unsteady discharges are considered. We confirmed our findings by comparing them with a more refined physically based model (Zolezzi & Seminara, 2001), as discussed and shown in the Supporting Information S1.

The HIPS model is rooted in a linearized treatment of the shallow water equations, and its main assumption is that the bank erosion rate, V, is proportional to the excess velocity at the river banks, u_b, through an erodibility coefficient E (Parker & Andrews, 1986). The excess bank velocity $u_b(s)$—where s is the curvilinear abscissa of the river centerline—is the local and linear perturbation of the depth-averaged velocity at the banks with respect to the uniform solution. After some algebra (Edwards & Smith, 2002), the main model outcome $V(s)$ parametrically depends on a spatial scale D, a temporal scale T and a pure number $\mathcal{P}$ (called the Parker number after Edwards and Smith (2002)) that respectively read

$$D = \frac{H}{2C_f}, \qquad T = \frac{D^2}{bEU}, \qquad \mathcal{P} = \frac{F^2 + A}{2}, \qquad (1)$$

where H and U are the reach-averaged depth and velocity, C_f is the friction coefficient (dependent on sediment roughness and depth), b is the channel half-width, F is the Froude number, and A is an empirical slope factor (Text S1, Supporting Information S1). Some remarks are in order: (a) the scale D emerges from shallow water equations and is the characteristic length scale of the backwater curve in open channel flows; (b) the timescale T is related to the bank erosion, so it is of the order of years or longer; (c) due to the meander elongation, the planform sinuosity S

changes in time and, consequently, so do the length and time scales according to $D = D_0 S^{1/3}$ and $T = T_0 S$, where D_0 and T_0 correspond to $S = 1$ (i.e., straight channel conditions, henceforth referred to with subscript zero); and (d) when dealing with unsteady flows, we also consider the change in the reach-averaged depth and velocity. To simplify the analysis, we instead assume the width to remain constant according to an idealized rectangular section.

The simulations are performed for three gravel-bed rivers with morphodynamic parameters representing real meandering rivers in the most likely sub-resonant regime (Seminara et al., 2024; Zolezzi et al., 2009)—that is, width-to-depth ratio not too large, see Zolezzi and Seminara (2001); Seminara (2006); Gautier et al. (2007)—and increasing formative flow (hence, increasing length scale D_0—see Table S1 in Supporting Information S1). The choice of the parameters fulfills literature formulas for hydraulic geometry under uniform flow conditions (Parker et al., 2007) (details are reported in Text S2, Supporting Information S1).

For each river, three configurations characterized by the same morphodynamic parameters but different flow conditions are explored. The first one adopts a steady (constant) discharge Q_{st} that induces the lateral migration of the river and corresponds to the one defining the river geometry (Text S2, Supporting Information S1). The other two configurations involve a variable flow Q_{unst} in which the stream velocity and depth are updated following the varying discharge at every timestep of the evolution, thus affecting also the sinuosity-dependent length and time scales governing the meandering dynamics (D and T, see Text S1, Supporting Information S1). The variability is simulated by randomly extracting a discharge value at any time step $Q(t)$ from a Gamma-shaped flood hydrograph. The rationale is that, when simulating discharge time series through a stochastic process resembling a random flood hydrograph with a Compound Poisson Process (CPP), the probability density function (PDF) results Gamma-distributed and this has shown to be a parsimonious and robust strategy in fluvial hydrology (Ridolfi et al., 2011). Although the CPP is a correlated process, the natural time correlation of discharge (order of months) is much shorter than the morphodynamic timescale of river meandering (order of decades/centuries), so some preliminary tests revealed that the temporal autocorrelation has no significant effects. For this reason, we here adopt only uncorrelated Gamma-distributed signals. In particular, at every timestep we extract a discharge that induces a lateral migration (i.e., Shield stress greater than its critical value)—thus overcoming the time-rescaling issue arising in other approaches, for example, the intermittency factor (Paola et al., 1992).

For the sake of comparison, we consider the mean of the variable-flow PDF equal to the discharge of the steady state, Q_{st}. The PDF variance, which is a proxy for flow unsteadiness, can be varied by adjusting the coefficient of variation while maintaining the same mean value. For each parametric setting (i.e., fluvial scenario), the following three cases are compared: $C_v = 0$ (steady flow Q_{st}), $C_v = 0.4$ and $C_v = 0.75$ (unsteady flows Q_{unst}). In the figures, these scenarios are reported with solid, dashed, and dotted lines, respectively.

Figure 1a shows the temporal evolution of the reach-averaged dimensionless curvilinear wavelengths λ_c, that is, twice the curvilinear distance between inflection points of the centerline (zero curvature). For comparison purposes, the wavelengths and times have been non-dimensionalized with the characteristic scales D_0 and T_0. The temporal behavior of λ_c highlights a first remarkable and counter-intuitive result: discharge variability slows down the meander growth (i.e., the same λ_c values are reached at longer times) with respect to the case of constant discharge. We identify four characteristic phases (colored shaded background in Figure 1a). In the beginning, when the wavelength has not yet been selected because the noise in the planimetry has just started to trigger the instability, all simulations are aligned, and the sinuosity is $S \simeq 1$ (phase 1). Then, the river starts selecting its typical wavelength, and the sinuosity slightly increases, resulting in an enhanced mean curvilinear wavelength (phase 2). In this phase, namely at $t/T_0 = 1-5$, the differences among the simulations are negligible. This phase is still characterized by linear processes with only weak perturbations to the planimetric evolution of the rivers (the average sinuosity for all the cases is still around $S \simeq 1.001$; see also planimetry A in Figure 1c). In this linear phase, flow variability yields the same mean meander wavelength as constant discharge (corresponding to the mean discharge of the unsteady case). The third phase, associated with the meander growth, completely changes the game. The discrepancy between the steady and unsteady cases bursts out as the meanders grow in both the curvilinear wavelength and sinuosity. The delayed evolution of the meanders forced by Q_{unst} is clear, and the time lag between the two cases accumulates the more the nonlinearities drive the curve growth dynamics in this phase. Finally, the fourth phase is dominated by the occurrence of cutoff events, a strongly nonlinear process by definition. They produce a saturation in the growth of the meanders and a long-term filtering action, resetting the system's memory (Camporeale et al., 2008). Note that we have slightly overlapped the regions characterizing phases 3 and 4 due to the different time scales of the three rivers.
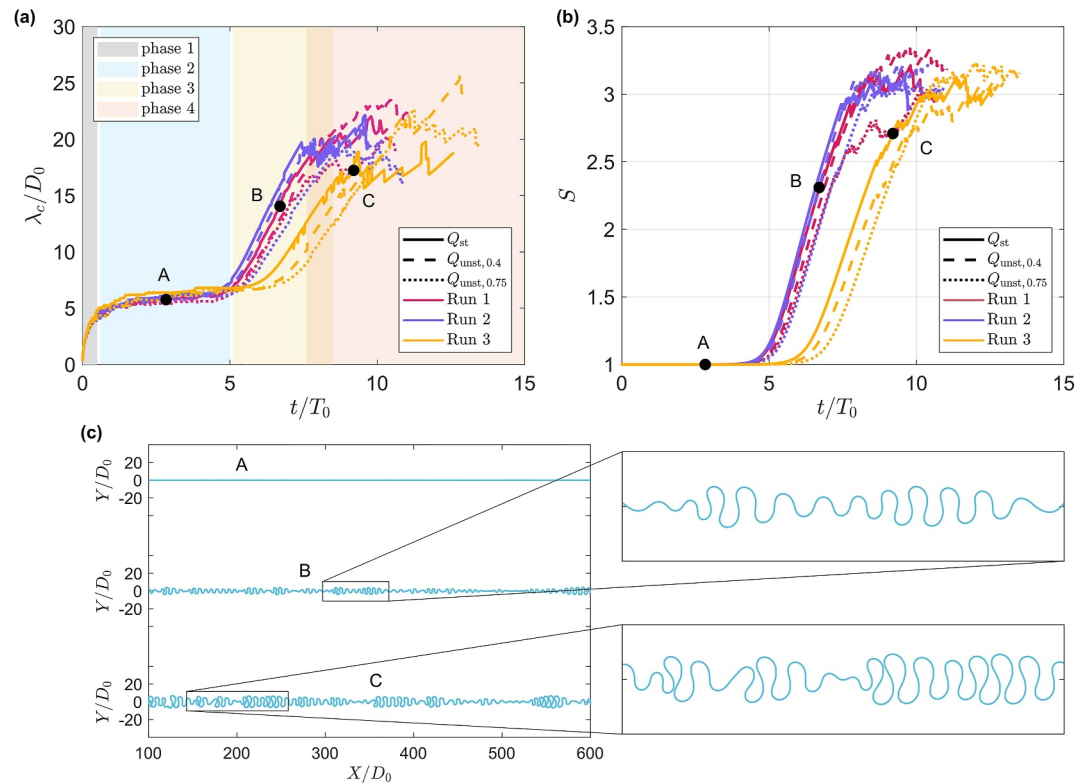
Figure 1. Impact of flow unsteadiness on simulated meander growth. Time series of (a) the dimensionless reach-averaged curvilinear meander wavelength λ_c/D_0 and (b) the river sinuosity S. The colors code the three simulated rivers set (Table S1, Supporting Information S1), while line styles indicate flow conditions: solid for steady discharge Q_{st}, dashed and dotted for varying discharges (Q_{unst}) with coefficients of variation of 0.4 and 0.75, respectively. The shaded areas in panel (a) qualitatively highlight the four phases described in Sect. 2, with a focus on the corresponding river planimetries (black dots) reported in panel (c).

The behavior of λ_c is mirrored in the river sinuosity S, that is, the ratio between the curvilinear length and the linear distance between its endpoints (Figure 1b). The temporal evolution of S confirms that the discharge variability slows down the meandering growth. In each Run, the sinuosity of the constant flow simulation starts growing earlier than that of Q_{unst}. Namely, the meander bends develop faster without discharge fluctuations. The first sinuosity drops due to cutoff events, which put an end to the simulations, are also delayed when flow unsteadiness occurs. Notice that the delay in morphological dynamics induced by flow unsteadiness is greater the larger the coefficient of variation, C_v, so confirming that the shift in the meander growth is linked to the variability itself.

3. Mathematical Analysis and Interpretation

Three key features have emerged from the above numerical simulations: (a) flow variability does not significantly affect the wavelength selection during the first (linear) phases (1 and 2) of the meandering dynamics, (b) different wavelengths appear over medium-long times (phases 3 and 4), and (c) discharge fluctuations induce a meander-growth slowdown that is evident throughout the dynamics. Here, we provide explanations and insights into these results by physically based analyses. Specifically, the linear component of meandering dynamics helps to understand the initial meander-growth phases, while nonlinear components are critical during later stages.

3.1. Linear Dynamics

A long tradition of modeling has shown that the inception of river meandering is nicely described by analytically manageable linear approaches (Camporeale et al., 2007). At the initial stages of the dynamics, when the river sinuosity is still very low, a classical linear stability analysis of the evolution equation of a simple harmonic planform provides the so-called dispersion relationship, relating the temporal growth rate σ, the wavelength λ and

some relevant governing parameters (e.g., for the HIPS model the parameters listed in Equation 1, see also Supporting Information S1, Text S1). By focusing on the role of the water depth H—that is, the fluctuating forcing of the present problem, being H dependent on Q—the dispersion relationship has a general form $\sigma = \sigma(\lambda, H)$. A contour plot of σ, for the model HIPS, is reported in Figure 2a, and it is crucial to understand phases 1 and 2 of the numerical simulations. The figure also reports the fastest-growing mode (black line) associated with any flow depth, namely the value λ_s such as $\sigma(\lambda_s)$ is maximum for a given depth. Notably, for a given planimetric configuration (fixed value of λ), the meander growth rate in the proximity of the fastest-growing mode decreases with higher flow depth values. Namely, higher flows slow down the meander growth and can even reverse it (gray region of Figure 2a). The physical reason is that, when the depth increases, the lateral superelevation of the free surface increases, with a damping effect on secondary currents and bed shoaling at the outer bank, so reducing lateral bank erosion.

A crucial aspect is the quasi-linear dependence of the fastest-growing mode on the flow depth. Since the dynamics are linear (thus, the superposition principle is valid), the nearly straight shape of the plot $\lambda_s = \lambda_s(H)$ implies that the average wavelength, forced by random water depths (PDF $p(H)$ shown in Figure 2b), is close to the wavelength corresponding to the mean depth $\bar{H}$. In fact, the probability-weighted (linear) growth rate $\bar{\sigma}(\lambda) = \int \sigma(\lambda, H)p(H)dH$ peaks nearly at the same wavelength selected in the steady deterministic case with $H = \bar{H}$ (Figure 2c). This explains why in the simulations, as long as the dynamics are linear (i.e., phases 1 and 2), rivers exhibit the same typical wavelength regardless of depth fluctuations, being the (constant) water depth of the deterministic case equal to the mean of the Gamma-distributed temporal series ($\bar{H}$).

A second and more subtle aspect emerges. Each water depth tends to select the wavelength λ_s performing the maximum growth. For example, in the constant flow case ($H = \bar{H} = 3$ m in Figure 2a), the selected wavelength is around $\lambda_s|_{H=3} = 1900$ m, and the typical time scale is $\tau = 2\pi/\sigma \sim 120$ years. However, in the varying flow case depths change over time and the linear wavelength selection mechanism adjusts continuously. The two red paths reported in Figure 2a provide possible scenarios. The path from point A to C describes an increase in water depth (H from 3 to 4 m), with two consequences on the system: (a) a first rapid response (A→B) induced by the new water current ($H = 4$ m) flowing in the planimetry and having wavelength $\lambda_s|_{H=3}$ selected by $H = 3$ m. This results in a reduction of the growth rate σ, that changes from $\sigma(\lambda_s|_{H=3}, H = 3) = 0.05$ to $\sigma(\lambda_s|_{H=3}, H = 4) = 0.02$; (b) a second slow response (B→C), that is the wavelength selection adjustment which gradually brings the wavelength to the new value of $\lambda_s|_{H=4} \simeq 2800$ m (on the black line) and to the growth rate $\sigma(\lambda_s|_{H=4}, H = 4) = 0.02$. This path A–B–C therefore implies a slowdown of growth. Differently, reducing the water depth from 3 to 2 m (path A–B′–C′) performs an opposite picture: both rapid and slow responses entail a greater growth rate compared to the starting condition with $H = 3$ m. The key point explaining the overall slowdown of meandering dynamics observed in the simulations is that a large region of the domain exhibits low or negative growth rates. Therefore, a 'slowdown effect' seems generally to prevail when discharge fluctuations induce H to move over the entire domain.

A definitive proof of such a prevalence is provided by the computation of the probability-weighted function $\bar{\sigma}(\lambda) = \int \sigma(\lambda, H)p(H)dH$ where, for a given value of λ, the growth rate is weighted with the PDF of the depth (see yellow line in Figure 2c). It clearly emerges that this function is sensibly lower than the growth rate computed with the average depth (i.e., $\sigma(\lambda, H = \bar{H})$, blue line in Figure 2c). In particular, both functions peak at almost the same wavelength, but the peak value of the former is about 30% smaller than the latter. Finally, notice that the same slowdown effect occurs if other (realistic) water depth PDFs (e.g., exponential, log-normal) or more advanced meandering models (e.g., by Zolezzi and Seminara (2001)) are taken into account. It follows that the stochasticity-induced delay with respect to the constant-discharge case is not model-specific, but it is peculiar to the meandering dynamics.

3.2. Nonlinear Dynamics

Geometrical nonlinear effects come into play as the river plan evolves and the meanders grow in sinuosity. To understand the role of the (geometric) nonlinearities in the slowdown effect under unsteady conditions, we consider a realistic prototype of channel planimetry, known as Kinoshita's curve (Parker & Andrews, 1986). The curve representation is based on the local tangent angle with respect to the downslope direction, given in terms of the curvilinear coordinate s, as in
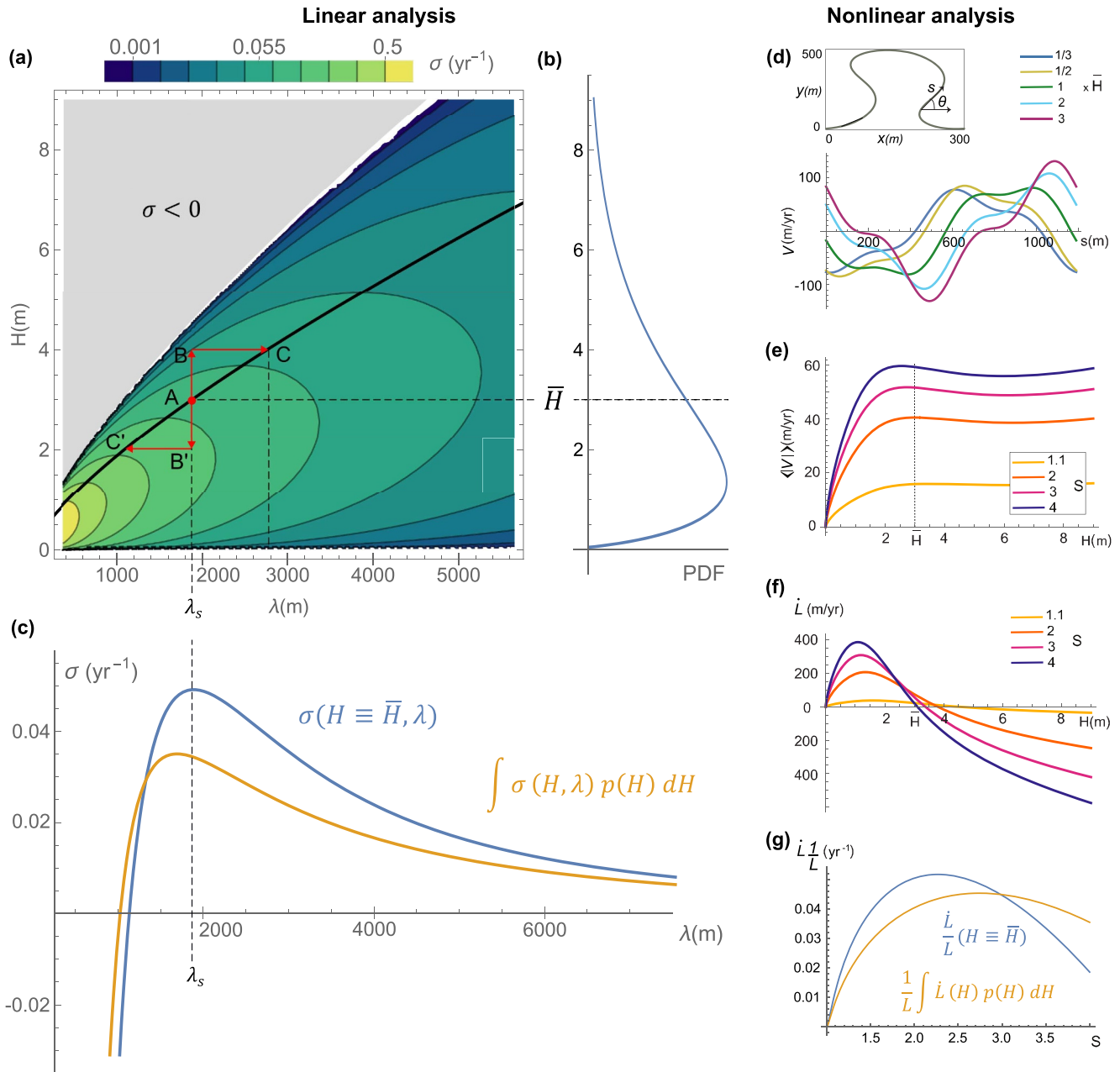
Figure 2. Linear (a)–(c) and nonlinear (d)–(g) analyses. (a) Contour plot of the linear growth rate σ as a function of the meander wavelength (λ) and flow depth (H). The solid black line marks the fastest-growing wavelength for any given water depth, while red arrows indicate the paths A–B–C and A′–B′–C′ (details in the main text). (b) Example of PDF for the water depth ($C_v = 0.75$). The average flow depth ($\bar{H} = 3$ m) equals the flow depth in the deterministic case with constant flow. (c) Growth rate versus wavelength for the constant flow depth (blue line) and probability-weighted growth rate $\int \sigma(H, \lambda)p(H)\,dH$ for the varying flow case (yellow line). The vertical dashed line highlights the maximum growth rate selecting the emerging wavelength λ_s in the deterministic case. Note how the maximum growth rate in the varying flow case is much lower. (d) Local migration rate V along the meander for various flow depths as fractions or multiples of the time-averaged formative flow $(\bar{H})$. The box at the top shows the meander geometry obtained with the Kinoshita curve (Equation 2) for $S = 4$. (e) Wavelength-averaged migration rate $\langle |V| \rangle$, and (f) length change rate $\dot{L}$, as a function of the flow depth and for different meander sinuosities S. (g) Relative meander length change rates $\dot{L}/L$ for the average depth $\bar{H}$ (blue line) and integrated over the PDF of H (yellow line) as functions of the sinuosity S. In all the panels, the river parameters are: $b = 27$ m, $d_{50} = 0.03$ m, $E = 10^{-6}$, and slope $J = 0.43\%$.

$$\theta(s) = \epsilon \sin(qs) + \frac{\epsilon^3}{64}\left[\sqrt{\mathcal{P}} + \cos(3qs) + \frac{1}{3}\sin(3qs)\right], \tag{2}$$

where ϵ is the meander amplitude, related to sinuosity through the polynomial $S^{-1} = 1 - \epsilon^2/4 + \epsilon^4/64 - \epsilon^6/2304$ (Edwards & Smith, 2002), and $q = 2\pi/\lambda$ is the curvilinear wavenumber. By introducing Equation 2 in the HIPS model (see Equation 3 in Supporting Information S1, Text S1) and assuming periodic boundary conditions, $V(s) = V(s + 2\pi/q)$, one obtains the migration velocity along the meander

$$V(s) = \alpha_5 U[\alpha_1 \cos(qs) + \alpha_2 \cos(3qs) + \alpha_3 \sin(qs) + \alpha_4 \sin(3qs)], \qquad (3)$$

where the coefficients α_i are reported in Text 3 of Supporting Information.

Figure 2d shows the migration rate $V(s)$ for a Kinoshita-meander planimetry characterized by a relatively high sinuosity ($S = 4$) for different water depths. Two important nontrivial features emerge: (a) the structure of the function $V = V(s)$ is highly dependent on the flow characteristics, with peaks occurring at different points along the meander, depending on the water depth; (b) although the peak values of $V(s)$ can increase with depth, this is not generally true for large portions of the meander, where migration rates not ordered according to the water flow are observed.

The response of the meander migration rate to different flow rates has very interesting consequences for both the wavelength-averaged migration rate, $\langle|V|\rangle = (q/2\pi) \int_0^{2\pi/q} |V| ds$, and the rate of meander length change, $\dot{L} = \int_0^{2\pi/q} V(d\theta/ds) ds$ (see Text S3, Supporting Information S1 for the analytical solution). The non-obvious behaviors of these quantities are shown in Figures 2e–2g. The average migration rate $\langle|V|\rangle$ is not a monotonously increasing function of the flow, but it has a maximum at low-medium depth values that becomes more evident at higher sinuosities. That is, the greater discharges can give rise to high local values of migration (see peaks in Figure 2d), but they are not responsible for the greater global planimetric movements along the entire meander. This counter-intuitive result is confirmed by looking at the relation between the meander length change and the flow depth for different sinuosities, $\dot{L} = \dot{L}(H, S)$ (Figure 2f). $\dot{L}$ increases with the sinuosity but depends on the water stage to a great extent. $\dot{L}$ is higher for low flows and becomes negative for high flows when the spatial distribution of the local migration velocity, V, is such that the meander tends to straighten back. In other words—before imposing their typical wavelength—high discharges have a straightening effect on the pre-existing plan (i.e., harmonic damping).

To clarify whether the acceleration of low flows or the dampening of higher flows is stronger in the nonlinear meander dynamics, we integrate $\dot{L}$ over the range of flow depths and compare it to the $\dot{L}$ obtained for a fixed, average flow—basically extending the linear stability analysis for σ (Figure 2a) to the finite-amplitude meanders. The results (Figure 2g) show an interesting regime shift as a function of the meander sinuosity. A meander with a low sinuosity evolves slower with variable flows, as expected from the linear analysis results. By contrast, a well-developed meander with a high sinuosity evolves faster with variable flows, meaning that the acceleration induced by low flows prevails over the dampening of the high flows. The location of the regime transition (namely the intersection between the two curves in Figure 2g) depends on the combination of hydrological and morphological parameters such as the PDF of H and the meander geometry, suggesting that location-specific analyses are necessary to assess the impact of flow variability on well-developed meanders.

4. Discussion and Conclusions

The comparison between the short-term evolution of meandering rivers under variable and constant flows has yielded several unexpected and counter-intuitive results. As often happens with nonlinear natural systems, the presence of noise leads to nontrivial phenomena. In this study, the noise is represented by the varying discharges, which play quite a surprising and unforeseen role in highly nonlinear complexities like meandering rivers. The most unpredictable effects are summarized here. Firstly, flow variability slows down both the formation and the evolution of meanders, resulting in a reduced sinuosity and average growth rate than the case under constant flow. In addition, the reach elongation induced by the local bank erosion is delayed, and such delay increases with time as the evolution proceeds. Finally, the meander length and the mean migration velocity decrease with high flow values.

In this context, it is worth discussing these outcomes in light of several implications upon the common knowledge of rivers, their management and flow regulation. Our analyses suggest that meandering rivers can experience a
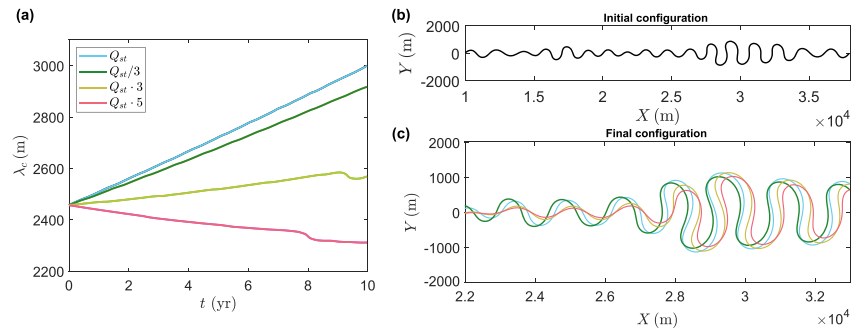
Figure 3. Evolution of a given river meander geometry for different flow values. (a) Evolution of the river-averaged curvilinear wavelength λ_c for the 4 cases reported in the legend ($Q_{st} = 500$ m³). (b) Initial planimetric configuration of the 4 simulations, that is, at time $t = 0$ years. (c) Zoom of the final configurations (at time $t = 10$ years); the color codes are the same as panel (a).

straightening process in the case of high flow to eventually set a different harmonic wave. A remarkable practical consequence is that a variation in the flow regime due to natural effects (e.g., climate-change induced droughts) or anthropogenic disturbance (e.g., dam regulation) can impact the existing meander wavelength. This aspect is further confirmed and investigated by numerical simulations shown in Figure 3. Starting from an already well-developed planimetry where the typical linear wavelength has already been selected, we investigate the impact of a sudden flow change on the meander curvilinear wavelength. Both lower and higher values of the flow (colored curves in Figure 3a) lead to a substantial reduction in the growth rate of the meander compared to the steady flow that generated the initial planform (black curve in Figure 3b). Moreover, if the discharge is particularly high (pink line in Figure 3), the river experiences a straightening and a reduction in the meander curvilinear length. This arguably counter-intuitive result demonstrates that an increase in the flow rate does not necessarily cause an increase in sinuosity.

Another crucial issue regards the actual dominant (or 'formative') discharge to be considered for meandering rivers. Our outcomes suggest that two formative flows are needed to characterize the meander dynamics: one for the meander wavelength selection (i.e., the average water flow), and one that determines the evolution timescale, which is not coincident with the mean flow. This can be verified by comparing the evolution of sinuosity for: (a) a constant steady discharge Q_{st}; (b) the equivalent variable flow Q_{unst} with mean equal to the steady case and degree of unsteadiness set to $Cv = 0.75$; and (c) a constant steady discharge slightly higher than Q_{st}. We observe that there is a steady flow (case (c) in this example) providing a temporal evolution of the sinuosity very close to the unsteady case (Figure S2, Supporting Information S1). Particularly, the value of the constant discharge that should be set in order to describe, as closely as possible, the timing of the meandering dynamics in the unsteady case is actually higher than the mean of the varying flow. This implies that the value adopted in numerical simulations running with a constant discharge should be chosen carefully and that the so-called formative discharge takes on different values depending on which aspect of the meandering dynamics one focuses on.

Along these lines, one wonders whether the choice of the numerical model (and so of the meandering features that it is capable of capturing) may affect such statements. We have therefore verified that the same outcomes emerge with a more advanced model proposed by Zolezzi and Seminara (2001) (Supporting Information S1). Although it takes into account features that are instead neglected in the HIPS model (e.g., secondary currents and sediment transport), the same conclusions are found with both models (Supporting Information S1, Figure S1). This suggests that the slowing down induced by varying flows is not imputable to sediment transport phenomena nor to modeling artifacts, but is a physical feature of the meander dynamics.

A final relevant remark concerns bank erodibility (E). This parameter depends on the history of the planform evolution process, the riparian vegetation, geological constraints, and anthropogenic effects (Seminara, 2006). As such, in this study, we adopted a typical literature value for E, resulting from field campaigns under the assumption of constant discharge (Parker & Andrews, 1986). For example, it was found that the erodibility coefficient mainly depends on bank material properties (C. Constantine et al., 2009) and, therefore, it seems that it can be estimated directly from field data without any assumptions on the controlling conditions, namely the forcing discharge(s). This implies that the choice of E implicitly accounts for an (historical) morphodynamic

evolution, where discharges have naturally varied and shaped the considered planform according to unsteady timescales. Thus, our study may open a debate around the proper steady discharge to be considered when testing in-situ conditions for the calibration of E. Of course, future work is needed to address and verify this hypothesis.

To conclude, we acknowledge that our current modeling approach operates under the assumption of a constant channel width. Although curvature nonlinearly induces width oscillations, and meandering rivers typically exhibit periodic planform sequences (Zolezzi et al., 2012), this assumption remains suitable for capturing discharge variability. Indeed, under varying flow conditions, Asahi et al. (2013) observed an overall equilibrium between bank erosion, leading to channel expansion, and land accretion, resulting in channel narrowing. Consequently, channel width remains nearly constant throughout the studied evolution.

It is important to note that many other factors contributing to river dynamics' complexity and fascination were not addressed in this study. These factors include, for example, temporal variations in river transects due to different flow regimes, interactions with vegetation dynamics, and soil heterogeneity. However, the findings presented here clearly demonstrate that flow fluctuations can induce non-trivial noise-induced phenomena, with significant implications for river engineering and the way rivers respond to changes in hydrological forcing.

Data Availability Statement

The Matlab code for the numerical simulations is available at Bassani and Camporeale (2024).

References

Asahi, K., Shimizu, Y., Nelson, J., & Parker, G. (2013). Numerical simulation of river meandering with self-evolving banks. *Journal of Geophysical Research: Earth Surface*, *118*(4), 2208–2229. https://doi.org/10.1002/jgrf.20150

Bassani, F., & Camporeale, C. (2024). Camporeale_Bassani_MEANDER-CODE-v1.0.0 [Software]. *Zenodo*. Retrieved from https://doi.org/10.5281/zenodo.11639091

Bertagni, M. B., Perona, P., & Camporeale, C. (2018). Parametric transitions between bare and vegetated states in water-driven patterns. *Proceedings of the National Academy of Sciences*, *115*(32), 8125–8130. https://doi.org/10.1073/pnas.1721765115

Buijse, A. D., Coops, H., Staras, M., Jans, L., Van Geest, G., Grift, R., et al. (2002). Restoration strategies for river floodplains along large lowland rivers in Europe. *Freshwater Biology*, *47*(4), 889–907. https://doi.org/10.1046/j.1365-2427.2002.00915.x

Camporeale, C., Perona, P., Porporato, A., & Ridolfi, L. (2005). On the long-term behavior of meandering rivers. *Water Resources Research*, *41*(12). https://doi.org/10.1029/2005wr004109

Camporeale, C., Perona, P., Porporato, A., & Ridolfi, L. (2007). Hierarchy of models for meandering rivers and related morphodynamic processes. *Reviews of Geophysics*, *45*(1). https://doi.org/10.1029/2005rg000185

Camporeale, C., Perucca, E., & Ridolfi, L. (2008). Significance of cutoff in meandering river dynamics. *Journal of Geophysical Research*, *113*(F1). https://doi.org/10.1029/2006jf000694

Carlin, M., Redolfi, M., & Tubino, M. (2021). The long-term response of alternate bars to the hydrological regime. *Water Resources Research*, *57*(7), e2020WR029314. https://doi.org/10.1029/2020wr029314

Ciotti, D. C., Mckee, J., Pope, K. L., Kondolf, G. M., & Pollock, M. M. (2021). Design criteria for process-based restoration of fluvial systems. *BioScience*, *71*(8), 831–845. https://doi.org/10.1093/biosci/biab065

Constantine, C., Dunne, T., & Hanson, G. J. (2009). Examining the physical meaning of the bank erosion coefficient used in meander migration modeling. *Geomorphology*, *106*(3–4), 242–252. https://doi.org/10.1016/j.geomorph.2008.11.002

Constantine, J. A., Dunne, T., Ahmed, J., Legleiter, C., & Lazarus, E. D. (2014). Sediment supply as a driver of river meandering and floodplain evolution in the Amazon Basin. *Nature Geoscience*, *7*(12), 899–903. https://doi.org/10.1038/ngeo2282

Duan, J. G., & Julien, P. Y. (2005). Numerical simulation of the inception of channel meandering. *Earth Surface Processes and Landforms: The Journal of the British Geomorphological Research Group*, *30*(9), 1093–1110. https://doi.org/10.1002/esp.1264

Eccles, R., Zhang, H., & Hamilton, D. (2019). A review of the effects of climate change on riverine flooding in subtropical and tropical regions. *Journal of Water and Climate Change*, *10*(4), 687–707. https://doi.org/10.2166/wcc.2019.175

Edwards, B. F., & Smith, D. H. (2002). River meandering dynamics. *Physical Review E*, *65*(4), 046303. https://doi.org/10.1103/physreve.65.046303

Eekhout, J., Hoitink, A., & Mosselman, E. (2013). Field experiment on alternate bar development in a straight sand-bed stream. *Water Resources Research*, *49*(12), 8357–8369. https://doi.org/10.1002/2013wr014259

Eke, E., Parker, G., & Shimizu, Y. (2014). Numerical modeling of erosional and depositional bank processes in migrating river bends with self-formed width: Morphodynamics of bar push and bank pull. *Journal of Geophysical Research: Earth Surface*, *119*(7), 1455–1483. https://doi.org/10.1002/2013jf003020

François, B., Schlef, K., Wi, S., & Brown, C. (2019). Design considerations for riverine floods in a changing climate–a review. *Journal of Hydrology*, *574*, 557–573. https://doi.org/10.1016/j.jhydrol.2019.04.068

Gautier, E., Brunstein, D., Vauchel, P., Roulet, M., Fuertes, O., Guyot, J.-L., et al. (2007). Temporal relations between meander deformation, water discharge and sediment fluxes in the floodplain of the Rio Beni (Bolivian Amazonia). *Earth Surface Processes and Landforms*, *32*(2), 230–248. https://doi.org/10.1002/esp.1394

Gilvear, D. J. (1999). Fluvial geomorphology and river engineering: Future roles utilizing a fluvial hydrosystems framework. *Geomorphology*, *31*(1–4), 229–245. https://doi.org/10.1016/s0169-555x(99)00086-0

Guo, X., Chen, D., & Parker, G. (2019). Flow directionality of pristine meandering rivers is embedded in the skewing of high-amplitude bends and neck cutoffs. *Proceedings of the National Academy of Sciences*, *116*(47), 23448–23454. https://doi.org/10.1073/pnas.1910874116

Hall, P. (2004). Alternating bar instabilities in unsteady channel flows over erodible beds. *Journal of Fluid Mechanics*, *499*, 49–73. https://doi.org/10.1017/s0022112003006219

Hasegawa, K. (1977). Computer simulation of the gradual migration of meandering channels. In *Proceedings of the hokkaido branch* (pp. 197–202). Japan Society of Civil Engineering.

Howard, A. D., & Hemberger, A. T. (1991). Multivariate characterization of meandering. *Geomorphology*, *4*(3–4), 161–186. https://doi.org/10.1016/0169-555x(91)90002-r

Ikeda, S., Parker, G., & Sawai, K. (1981). Bend theory of river meanders. Part 1. Linear development. *Journal of Fluid Mechanics*, *112*(-1), 363–377. https://doi.org/10.1017/s0022112081000451

Imran, J., Parker, G., & Pirmez, C. (1999). A nonlinear model of flow in meandering submarine and subaerial channels. *Journal of Fluid Mechanics*, *400*, 295–331. https://doi.org/10.1017/s0022112099006515

Inglis, C. C. (1949). *The behavior and control of rivers and canals*. Research Publication No. 13 Central Water Power.

Jansen, P., Van Bendegom, L., Van Den Berg, J., De Vries, M., & Zanen, A. (1979). *Principles of River Engineering: The non-tidal alluvial river*. Pitman.

Johannesson, H., & Parker, G. (1989). Linear theory of river meanders. *River Meandering*, *12*, 181–213. https://doi.org/10.1029/wm012p0181

Ollero, A. (2010). Channel changes and floodplain management in the meandering middle Ebro River, Spain. *Geomorphology*, *117*(3–4), 247–260. https://doi.org/10.1016/j.geomorph.2009.01.015

Paola, C., Heller, P. L., & Angevine, C. L. (1992). The large-scale dynamics of grain-size variation in alluvial basins, 1: Theory. *Basin Research*, *4*(2), 73–90. https://doi.org/10.1111/j.1365-2117.1992.tb00145.x

Parker, G., & Andrews, E. D. (1986). On the time development of meander bends. *Journal of Fluid Mechanics*, *162*(-1), 139–156. https://doi.org/10.1017/s0022112086001970

Parker, G., Paola, C., Whipple, K. X., & Mohrig, D. (1998). Alluvial fans formed by channelized fluvial and sheet flow. I: Theory. *Journal of Hydraulic Engineering*, *124*(10), 985–995. https://doi.org/10.1061/(asce)0733-9429(1998)124:10(985)

Parker, G., Shimizu, Y., Wilkerson, G., Eke, E. C., Abad, J. D., Lauer, J., et al. (2011). A new framework for modeling the migration of meandering rivers. *Earth Surface Processes and Landforms*, *36*(1), 70–86. https://doi.org/10.1002/esp.2113

Parker, G., Wilcock, P. R., Paola, C., Dietrich, W. E., & Pitlick, J. (2007). Physical basis for quasi-universal relations describing bankfull hydraulic geometry of single-thread gravel bed rivers. *Journal of Geophysical Research*, *112*(F4). https://doi.org/10.1029/2006jf000549

Perucca, E., Camporeale, C., & Ridolfi, L. (2005). Nonlinear analysis of the geometry of meandering rivers. *Geophysical Research Letters*, *32*(3). https://doi.org/10.1029/2004gl021966

Pittaluga, M. B., & Seminara, G. (2011). Nonlinearity and unsteadiness in river meandering: A review of progress in theory and modelling. *Earth Surface Processes and Landforms*, *36*(1), 20–38. https://doi.org/10.1002/esp.2089

Ridolfi, L., D'Odorico, P., & Laio, F. (2011). *Noise-induced phenomena in the environmental sciences*. Cambridge University Press.

Seminara, G. (2006). Meanders. *Journal of Fluid Mechanics*, *554*(-1), 271–297. https://doi.org/10.1017/s0022112006008925

Seminara, G., Tambroni, N., & Lanzoni, S. (2024). *Theoretical morphodynamics: River meandering*. Firenze University Press.

Tubino, M. (1991). Growth of alternate bars in unsteady flow. *Water Resources Research*, *27*(1), 37–52. https://doi.org/10.1029/90wr01699

Vesipa, R., Camporeale, C., & Ridolfi, L. (2017). Effect of river flow fluctuations on riparian vegetation dynamics: Processes and models. *Advances in Water Resources*, *110*, 29–50. https://doi.org/10.1016/j.advwatres.2017.09.028

Welford, M. R. (1994). A field test of Tubino's (1991) model of alternate bar formation. *Earth Surface Processes and Landforms*, *19*(4), 287–297. https://doi.org/10.1002/esp.3290190402

Zolezzi, G., Luchi, R., & Tubino, M. (2009). Morphodynamic regime of gravel bed, single-thread meandering rivers. *Journal of Geophysical Research*, *114*(F1). https://doi.org/10.1029/2007jf000968

Zolezzi, G., Luchi, R., & Tubino, M. (2012). Modeling morphodynamic processes in meandering rivers with spatial width variations. *Reviews of Geophysics*, *50*(4). https://doi.org/10.1029/2012rg000392

Zolezzi, G., & Seminara, G. (2001). Downstream and upstream influence in river meandering. Part 1. General theory and application to overdeepening. *Journal of Fluid Mechanics*, *438*(13), 183–211. https://doi.org/10.1017/s002211200100427x